Research Square

Preprints are preliminary reports that have not undergone peer review.
They should not be considered conclusive, used to inform clinical practice,
or referenced by the media as validated information.

Analytical and Interlaboratory Evaluation of an Adapted Procedure for 210Pb Determination by Alpha Spectrometry in Mangrove Sediments

Josué Armando Hernández Fuentes

josuejh2204@gmail.com

University of El Salvador

Darwin Josué López Alvarenga

University of El Salvador

Oscar Armando Amaya Monterrosa

University of El Salvador

Rodrigo José Mundo Dueñas

Autoridad Salvadoreña del Agua

Research Article

Keywords: ^{210}Pb, ^{210}Po, alpha spectrometry, interlaboratory comparison, mangrove sediments, sediment accumulation

Posted Date: November 3rd, 2026

DOI: https://doi.org/10.21203/rs.3.rs-11269758/v1

License: This work is licensed under a Creative Commons Attribution 4.0 International License.
Read Full License

Additional Declarations: No competing interests reported.

ANALYTICAL AND INTERLABORATORY EVALUATION OF AN ADAPTED PROCEDURE FOR ^{210}Pb DETERMINATION BY ALPHA SPECTROMETRY IN MANGROVE SEDIMENTS

Josué Hernández[1], Darwin López[1], Óscar Amaya-Monterrosa[1], Rodrigo Mundo[2]

[1]Marine Toxins Laboratory, University of El Salvador (LABTOX-UES), San Salvador, El Salvador; josuejh2204@gmail.com (J. Hernández); dlopezalvarenga77@gmail.com (D. López); oscar.amaya@ues.edu.sv (O. Amaya-Monterrosa).

[2]Salvadoran Water Authority, San Salvador, El Salvador; rodrigomundo12@gmail.com (R. Mundo).

Correspondence: josuejh2204@gmail.com

Abstract

An adapted procedure for indirect ^{210}Pb determination through ^{210}Po alpha spectrometry in mangrove sediments was evaluated for analytical performance and interlaboratory comparability, including the influence of analytical differences on CF–CS-derived sediment accumulation rates. Analytical performance was assessed using blanks, minimum detectable activity, ^{209}Po recovery, and IAEA-412 reference material. Comparison of 46 sediment sections between LABTOX-UES and IAEA-MEL showed statistical compatibility for 80.4% of paired results. York regression indicated a slope compatible with unity but a significantly negative intercept, precluding complete analytical equivalence. Nevertheless, surface mass and sediment accumulation rates showed no significant interlaboratory differences, supporting the procedure under the evaluated conditions.

Keywords: ^{210}Pb; ^{210}Po; alpha spectrometry; interlaboratory comparison; mangrove sediments; sediment accumulation

Introduction

Lead-210 (^{210}Pb) is a naturally occurring radionuclide of the ^{238}U decay series, with a half-life of approximately 22.2 years. Atmospheric ^{210}Pb, produced from the decay of ^{222}Rn, is deposited in terrestrial and aquatic environments and becomes associated with mineral particles and organic matter. In sediments, its unsupported or excess component ($^{210}Pb_{ex}$) provides a temporal framework of approximately 100–150 years and is widely used to establish recent chronologies and estimate mass accumulation and sedimentation rates in lacustrine, marine, and coastal environments [1–4].

The activity of ^{210}Pb can be determined directly by gamma-ray spectrometry or indirectly through its daughter radionuclide, ^{210}Po, by alpha spectrometry once radioactive equilibrium between the two radionuclides has been established [5]. The latter approach provides high sensitivity for the determination of low activity concentrations in environmental samples, although it requires radiochemical processing prior to measurement [6,7]. Its analytical performance can be influenced by different stages of the procedure, including sample digestion, chemical separation and recovery of polonium from the sediment matrix, preparation of alpha sources by spontaneous deposition onto metallic discs, and subsequent measurement by alpha spectrometry [6–8]. The addition of an isotopic tracer, such as ^{209}Po, enables the chemical recovery of polonium to be monitored and potential losses during sample processing to be

accounted for. Consequently, the implementation or adaptation of a ^{210}Po-based procedure for the indirect determination of ^{210}Pb requires appropriate analytical controls, including instrumental background, procedural blanks, minimum detectable activity, chemical recovery, analysis of reference materials, and evaluation of measurement uncertainty [6–9].

Although the techniques used for ^{210}Pb determination are well established, their analytical performance may depend on the sample matrix, radiochemical procedure, detection technique, required sensitivity, and laboratory conditions. Cuesta et al. compared low-level gamma-ray spectrometry, alpha spectrometry through ^{210}Po, and Cherenkov counting through ^{210}Bi for the determination of ^{210}Pb in different environmental matrices, including sediments, and found no significant differences among the three methods, although alpha spectrometry provided the highest precision [10]. More recently, Dulanská et al. compared two separation procedures for ^{210}Pb determination and evaluated their performance in terms of accuracy, precision, and analytical efficiency [11]. These studies demonstrate the importance of experimentally evaluating the performance and comparability of analytical procedures rather than assuming equivalence solely on the basis of the radionuclide being determined or the measurement principle employed.

This issue becomes particularly relevant when ^{210}Pb activity profiles are subsequently used to establish sediment chronologies or calculate accumulation rates. Zaborska et al. compared ^{210}Pb determinations by alpha and gamma spectrometry in marine sediment cores and observed agreement between the activities obtained by both techniques within counting uncertainties, as well as good agreement between the resulting sediment accumulation rates [12]. At a broader scale, an IAEA interlaboratory comparison exercise involving laboratories from 14 countries showed generally satisfactory analytical performance in radionuclide determination but also identified difficulties in the complete application of ^{210}Pb sediment dating and emphasized the importance of obtaining reliable activity profiles before establishing chronologies [13]. A complementary interlaboratory exercise focused on modelling further demonstrated that the interpretation of ^{210}Pb profiles and the implementation of dating models can introduce additional variability into the resulting chronologies and accumulation rates [14]. These findings indicate that analytical comparability should be evaluated not only in terms of the measured ^{210}Pb activity concentrations but also by considering the potential influence of analytical differences on the derived sedimentary parameters.

In this study, a procedure for the indirect determination of ^{210}Pb through ^{210}Po alpha spectrometry was adapted to the equipment and analytical conditions available at the Marine Toxins Laboratory of the University of El Salvador (LABTOX-UES). The digestion stage was adapted from IAEA-TECDOC-1953 [15], whereas alpha-source preparation was based on the procedure described in RiO5 Method 16 [16]. The analytical performance of the adapted procedure was evaluated through the determination of instrumental background, procedural blanks, minimum detectable activity, ^{209}Po tracer recovery, and analysis of the IAEA-412 reference material. Its interlaboratory comparability was subsequently evaluated using 46 sections of a mangrove sediment core independently analyzed by LABTOX-UES and the IAEA Marine Environment Laboratories (IAEA-MEL). Finally, the influence of the analytical differences observed between the two laboratories on mass accumulation and sedimentation rates derived from the constant flux–constant sedimentation (CF–CS) model was evaluated.

MATERIALS AND METHODS

Preparation of Sediment Samples Prior to Digestion for ^{210}Pb Analysis

The sediment samples analyzed in this study were obtained from core Z3N5, collected in Jiquilisco Bay, El Salvador, by personnel from the Marine Toxins Laboratory of the University of El Salvador (LABTOX-UES), in coordination with the Salvadoran Water Authority (ASA) and the Ministry of Environment and Natural Resources (MARN), within the framework of the International Atomic Energy Agency (IAEA) ELS7011 project. The core was collected in September 2024 using the push-core technique with a PVC tube measuring 10 cm in internal diameter and 100 cm in length.

The sediment core was cut longitudinally to expose the sediment column and allow a visual description of its stratigraphic characteristics, including changes in color and texture, the presence of organic remains, and visible variations among strata. It was subsequently sectioned transversely at intervals defined according to depth: 1 cm between 0 and 20 cm, 2 cm between 20 and 50 cm, and 3 cm at depths greater than 50 cm [17].

Each section was placed individually in a previously labeled aluminum container, and its wet mass was recorded. The samples were dried in a Binder oven at 60 °C for 48 h. Completion of the drying process was verified by successive weighing of a reference sample, using a variation of less than 4% between two consecutive measurements as the stability criterion. The dry mass of each sample was then recorded, and the samples were stored individually in labeled Ziploc bags bearing their respective identification codes. Finally, the samples were homogenized and ground with an agate mortar until an approximate particle size of 300 µm was achieved (Fig. 1).

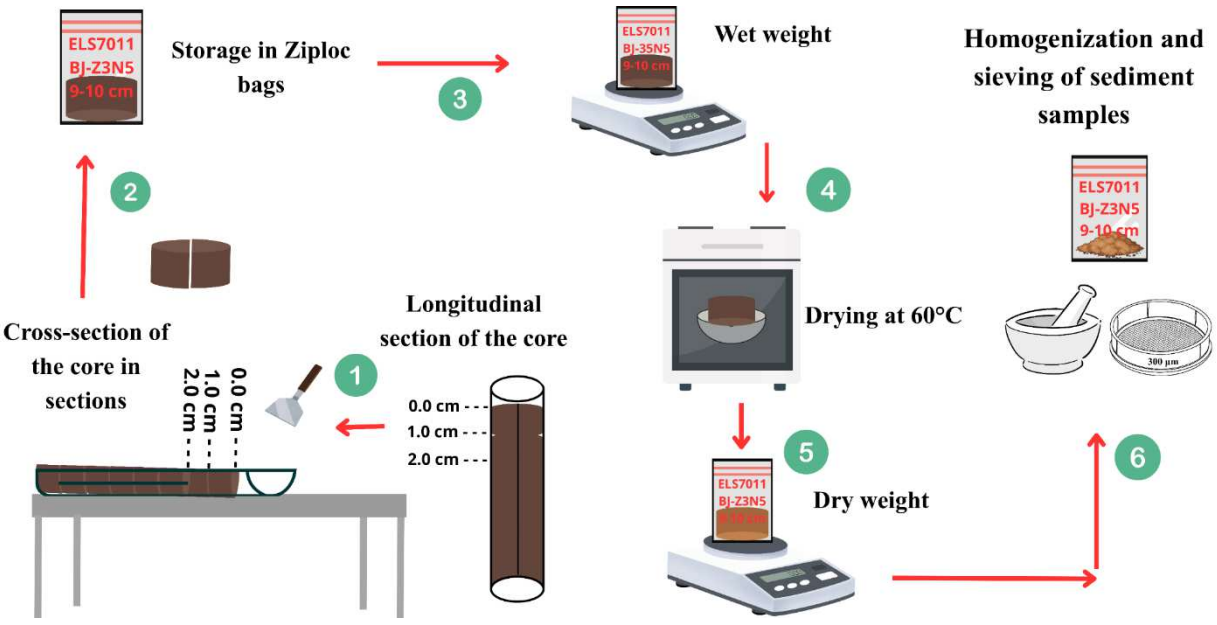


Fig. 1. Illustration of sample preparation prior to ^{210}Pb analysis by alpha spectrometry.

Thermal Gradient

To evaluate the thermal uniformity of the hotplate (IKA C-MAG HP 10), the temperature was set to 100 °C. This condition was selected to safely examine the spatial distribution of the surface temperature without placing containers holding samples or reagents on the hotplate. The purpose of the test was not to reproduce the internal temperature reached by the mixtures

during digestion, but to identify the surface regions exhibiting greater thermal uniformity and smaller deviations from the set temperature.

For this purpose, the 25.0 cm × 25.0 cm heating surface was divided into 25 square sections measuring 5.0 cm × 5.0 cm. This discretization allowed a specific and reproducible spatial position to be assigned to each digestion vessel during sample preparation. Each section was identified by a unique code corresponding to the digestion vessel positions (IDs 1–25) and arranged in a spatial matrix defined by the coordinates (x, y), where $x$and $y$represent the horizontal and vertical positions, respectively.

Based on this spatial distribution, the surface temperature of each section was measured using an infrared thermometer (Klein Tools IR5) at 10-minute intervals over a total period of 40 minutes to capture potential temporal variations in temperature. For the analysis, the median of the four measurements taken at different times was calculated for each hotplate position. Thus, the ANOVA included 25 independent spatial observations: nine corresponding to the central region and eight corresponding to each of the two peripheral groups. Successive measurements taken at the same position were considered repeated measurements and were therefore not treated as independent observations.

A one-way analysis of variance (ANOVA) was subsequently performed using the location zone of the digestion vessel as the only factor, classified into three levels: central region, peripheral group 1, and peripheral group 2, according to the spatial distribution shown in Fig. 2. This analysis was used to determine whether statistically significant differences in temperature existed among the three regions of the hotplate under the conditions of the thermal test.

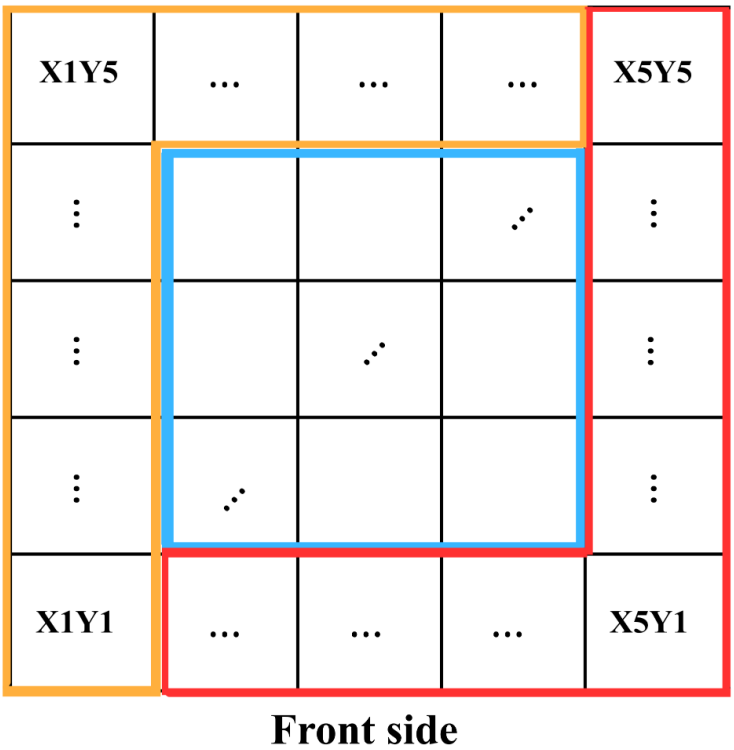


Fig. 2. Spatial distribution of the 25 positions defined on the heating surface of the hotplate (IKA C-MAG HP 10) for thermal characterization. The positions were classified into three zones: groups 1 and 2, shown in orange and red, respectively, and the central region of the hotplate, shown in light blue.

Determination of ^{210}Pb at LABTOX-UES

The methodology applied in this study was based on the integration of two complementary procedures. The first consisted of an acid digestion protocol using a hotplate, following the methodological parameters established in IAEA-TECDOC-1953 [15], including the types and volumes of acids used, heating temperature, and digestion time. The second was based on the methodology implemented at the International Atomic Energy Agency (IAEA) Marine Environment Laboratories in Monaco, as described in RiO5 Method 16 [16], for the preparation and deposition of ^{210}Po. Both procedures were adapted to the laboratory's operating conditions and available resources while maintaining the analytical principles and quality-control criteria established in the reference methods.

Fig. 3. Illustration of the steps involved in preparing sediment samples for digestion and subsequent ^{210}Pb analysis by alpha spectrometry.

^{210}Pb activity in the sediment samples was determined indirectly through its daughter radionuclide ^{210}Po by alpha spectrometry, using ^{209}Po as an isotopic tracer to determine the chemical recovery of the procedure. For each analysis, approximately 0.30 g of previously dried, homogenized, and ground sediment was weighed. As part of the analytical quality control, a procedural blank and the IAEA-412 certified reference material (Pacific Ocean marine sediment) were included.

A 300 µL aliquot of a ^{209}Po tracer solution (Eckert & Ziegler Isotope Products) was added to each sample, and the mass added was recorded. The tracer solution was refrigerated at 4 °C and, before use, was allowed to equilibrate at room temperature for approximately 1 h to prevent condensation during handling.

For digestion, 5 mL of nitric acid (HNO_3, 65%, NF grade, J.T. Baker™), 4 mL of hydrochloric acid (HCl, 37%, ACS analytical reagent grade, EMSURE®, Merck), and 1 mL of hydrofluoric acid (HF, 48%, ACS reagent grade, RGH) were added to each sample. This mixture facilitated the oxidation of organic matter and the dissolution of the main carbonate and silicate phases present in the sedimentary matrix. After the reagents were added, the digestion vessels were tightly sealed and placed on a hotplate (IKA C-MAG HP 10) at 150 °C for at least 16 h (Fig. 3).

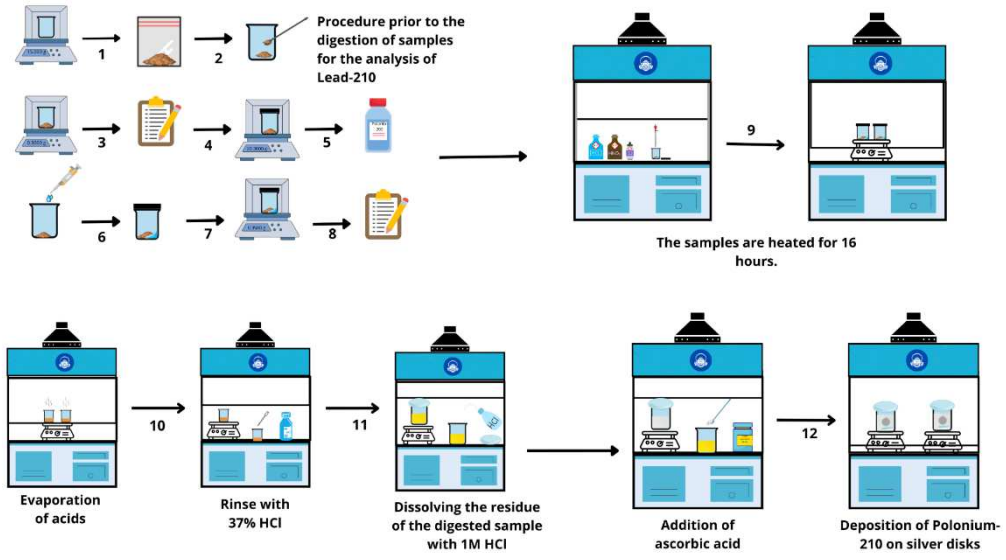


Fig. 3. Illustration of the steps involved in preparing sediment samples for digestion and subsequent ^{210}Pb analysis by alpha spectrometry.

After digestion was completed, the vessels were opened and their caps were carefully rinsed with 1 M HCl to minimize sample loss. The vessels were returned to the hotplate (IKA C-MAG HP 10), and the acid mixture was evaporated at 70–80 °C. During this stage, the temperature was maintained below 90 °C to minimize potential losses of ^{209}Po and ^{210}Po through volatilization. Once evaporation was complete, 2.5 mL of concentrated HCl was added to each vessel, and the contents were again evaporated to dryness. This procedure was performed twice to remove residual acids and condition the medium for the subsequent deposition of polonium onto silver discs. The resulting residue was redissolved in approximately 30 mL of 1 M HCl and maintained at 70–80 °C for several minutes. The solution was then quantitatively transferred into previously labeled 150 mL beakers, using 1 M HCl to rinse the digestion vessels and ensure complete transfer. The final volume was adjusted to 100 mL with 1 M HCl, and the solutions were maintained at 70–80 °C on a stirring hotplate (IKA RT10 S001).

Before polonium deposition, 50 mg of ascorbic acid was added to each sample to reduce Fe^{3+} to Fe^{2+} and minimize potential interference during the spontaneous deposition of polonium. The silver discs were perforated near their outer edges and suspended in the solutions using approximately 32 cm of nylon thread. The samples were stirred at 400 rpm for 14 h at 70–80 °C to promote the spontaneous deposition of ^{209}Po and ^{210}Po onto the surfaces of the silver discs. Upon completion of the process, the discs were removed, carefully rinsed with Milli-Q water, and stored individually in previously labeled envelopes until alpha spectrometric analysis. Finally, the activities of ^{209}Po and ^{210}Po deposited on the discs were determined by alpha spectrometry using an ALPHA DUO system (ORTEC AMETEK) equipped with passivated implanted planar silicon (PIPS) detectors.

Alpha Spectrometer Calibration and Background Measurement

The measurement system was calibrated using individual americium-241 and plutonium-239 standard sources manufactured and certified by Eckert & Ziegler, with energies of 5.486 and 5.157 MeV, respectively, according to data from the *IAEA Nuclear Data Services*. The sources were individually positioned at a fixed distance of approximately 5 mm from the active surface of the PIPS detector under vacuum conditions below 500 mTorr. The characteristic alpha peaks of each radionuclide were identified from the resulting spectra, and the channel–energy relationship was established by assigning the reference energies to their corresponding channels and assuming a linear response of the system. The instrumental background was measured using a counting time equivalent to that employed for the samples. This measurement was performed using blank silver discs.

Detector efficiency was not determined using the americium-241 (^{241}Am) and plutonium-239 (^{239}Pu) sources because these sources have a thickness of 3.18 mm and an active-area diameter of 5 mm, whereas the discs used in this study have a thickness of 0.70 mm and an active-area diameter of 22 mm. This geometric discrepancy precluded direct determination of the system efficiency because the source-to-detector geometry of the calibration sources differed from that of the analyzed samples. Given the relevance of this limitation, the mean solid angle subtended by a circular source at the detector was calculated, as illustrated in Fig. 4.

Based on the approach developed by Gascón and Muñoz [18], a geometric expression was obtained using an infinite-series approximation truncated after the first three terms, as shown in Eq. (1).

$$\langle \varepsilon \rangle = \frac{1}{2}\left[\frac{R_D^2}{D(D+H)}\right] - \frac{3}{16}\frac{R_S^2 R_D^2 H}{D^5} + \frac{5}{32}\frac{R_S^4 R_D^2 H}{D^9}\left[H^2 - \frac{3}{4}R_D^2\right] \quad (1)$$

Based on this expression, the efficiency was calculated using a source-to-detector distance of 4 mm, corresponding to the geometry employed during the measurements. Under these experimental conditions, the estimated efficiency was approximately 29% for each detector.

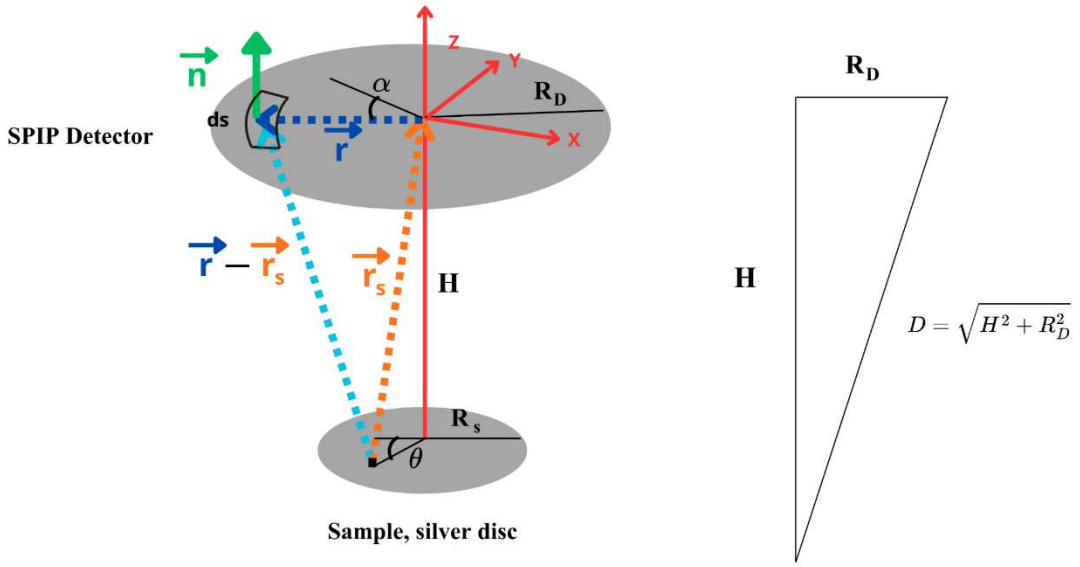


Fig. 4. Geometric diagram of the source–detector arrangement used to estimate alpha spectrometry efficiency through the solid-angle approach developed by Gascón and Muñoz [18].

Determinación de la actividad de ^{210}Pb

The activity of ^{210}Pb was determined indirectly through its daughter radionuclide ^{210}Po using the isotope-dilution technique, with ^{209}Po as a tracer. A known amount of tracer was added to each sample before the main stages of the radiochemical procedure, allowing the chemical recovery to be determined individually and correcting for polonium losses occurring during sample processing. The activity was calculated from the ratio of the net count rates of ^{210}Po and ^{209}Po, considering the activity and mass of the added tracer, the mass of sediment analyzed, blank and background contributions, and radioactive-decay correction factors according to [8]:

$$A\ (\mathrm{Bq\ kg^{-1}}) = \frac{A_T\, m_T}{m_A}\left[\frac{R_{GA}-R_{BA}}{R_{GT}-R_{BT}} - \frac{R_{GAb}-R_{BA}}{R_{GTb}-R_{BT}}\right] f_A\, f_T\, f_{\mathrm{Pb-210}} \qquad (2)$$

where $A$was the determined activity (Bq kg^{-1}); $A_T$was the specific activity of the ^{209}Po tracer (Bq g^{-1}); $m_T$was the mass of tracer added (g); and $m_A$was the mass of sediment analyzed (kg). R_{GA} and R_{GAb}were the ^{210}Po count rates in the sample and blank, respectively; R_{GT} and R_{GTb}were the ^{209}Po count rates in the sample and blank, respectively; and R_{BA} and R_{BT}were the background count rates in the ^{210}Po and ^{209}Po regions of interest, respectively. Finally, f_A, f_T, and $f_{\mathrm{Pb-210}}$were the decay correction factors applied to the analyte, tracer, and ^{210}Pb, respectively.

Interlaboratory comparison of ^{210}Pb determination

For conducting an interlaboratory comparison, the ^{210}Pb activity concentration in the sections of sediment core ELS7011-BJ-Z3N5 was determined at the International Atomic Energy Agency Marine Environment Laboratories (IAEA-MEL) in Monaco. The determination was performed indirectly by measuring its daughter radionuclide ^{210}Po using alpha spectrometry, following the procedure described in RiO5 Method 16, ERL-ECU/LM/0001-01 [16]. For each

determination, approximately 0.30 g of previously homogenized and sieved dry sediment with a particle size below 300 μm was weighed. The samples were transferred into TFM MARSXpress digestion vessels, and 200 μL of a ^{209}Po tracer solution was added to determine the chemical recovery and correct for polonium losses during radiochemical processing. Digestion was performed using a mixture of 9 mL of concentrated HNO_3 and 3 mL of concentrated HF in a CEM MARS 6™ microwave digestion system equipped with a 40-position MARSXpress rotor at 180 °C for 25 min. After digestion and cooling of the vessels, 15 mL of a boric acid solution was added to complex the residual fluoride and reduce the formation of insoluble fluorides.

The solution was subsequently evaporated to dryness at approximately 80 °C. The residue was redissolved in 2 mL of concentrated HCl and evaporated to dryness again. This acidification and evaporation process was repeated three times to remove residual acids and condition the sample for subsequent polonium deposition. The final residue was redissolved in 100 mL of 1 M HCl, and the solution was heated to 80 °C. Subsequently, 50 mg of ascorbic acid was added to reduce Fe^{3+} to Fe^{2+} and minimize its interference during deposition. Polonium isotopes were isolated by spontaneous deposition onto silver discs 2 cm in diameter, while the solutions were maintained under magnetic stirring for 8 h at 80 °C. Finally, the activities of ^{209}Po and ^{210}Po deposited on the discs were determined by alpha spectrometry using an ALPHA DUO system (ORTEC AMETEK) equipped with PIPS silicon detectors. The ^{210}Pb activity concentration was calculated from the ^{210}Po activity, assuming secular equilibrium between the two radionuclides, and was corrected for the individual recovery of the ^{209}Po tracer. To perform the interlaboratory comparison under the same reference conditions, the activity concentrations determined by both laboratories were decay-corrected to the sediment-core sampling date and expressed on a dry-mass basis.

Determination of supported ^{210}Pb and calculation of excess ^{210}Pb

The activity concentration of ^{226}Ra was determined by gamma spectrometry at the International Atomic Energy Agency Marine Environment Laboratories (IAEA-MEL), Monaco, using a well-type high-purity germanium (HPGe) detector identified as D70. Five sections of core ELS7011-BJ-Z3N5, corresponding to depths of 5, 16, 26, 36, and 46 cm, were analyzed. For the measurements, between 5.4384 and 5.9179 g of dry sediment were used and placed in containers corresponding to calibration geometry 6. Counting times ranged from 1.25–6.02 days. Before the measurements, the containers were sealed and left undisturbed for 22 days to promote the establishment of radioactive equilibrium between ^{226}Ra and its short-lived descendants following ^{222}Rn. The activity concentration of ^{226}Ra was estimated from the ^{214}Pb gamma lines at 295.21 and 351.92 keV, with emission probabilities of 19.2 and 37.2%, respectively.

For each section, the activity concentration corresponding to each line was calculated, and their mean was used as an estimator of ^{226}Ra activity. The ^{226}Ra activity concentrations determined in the five sections ranged between 7.87 ± 0.06 and 10.21 ± 0.46 Bq kg^{-1}. The arithmetic mean was 9.52 Bq kg^{-1}, with a standard deviation of 0.97 Bq kg^{-1} and a standard error of the mean of 0.43 Bq kg^{-1}. No significant linear trend was observed between ^{226}Ra activity and depth ($r = 0.25$; $p = 0.69$). Therefore, the mean value was used as a constant estimator of supported ^{210}Pb activity in the 46 core sections.

The excess ^{210}Pb activity concentration was calculated for each section as the difference between the total ^{210}Pb activity and the mean ^{226}Ra activity [19]:

$$A(^{210}\mathrm{Pb}_{ex}) = A(^{210}\mathrm{Pb}_{total}) - \bar{A}\,(^{226}\mathrm{Ra}) \qquad (3)$$

Statistical analysis and application of the CF–CS model

The analyses were performed using Microsoft Excel and scripts developed in Python with the NumPy and SciPy libraries. Excel was used for descriptive statistics and the one-way ANOVA applied to the hotplate zones, whereas Python was used for compatibility tests, correlation, regressions, and calculations derived from the CF–CS model. Measurement uncertainties were treated as standard uncertainties ($k = 1$), and a significance level of $\alpha = 0.05$ was adopted.

The compatibility between the activity concentrations determined by LABTOX-UES and IAEA-MEL was evaluated individually for each section using a z-statistic calculated from the difference between both results and their combined standard uncertainty [9]:

$$z_i = \frac{A_{\mathrm{LAB},i} - A_{\mathrm{IAEA},i}}{\sqrt{u^2_{\mathrm{LAB},i} + u^2_{\mathrm{IAEA},i}}} \qquad (4)$$

where $A_i$and $u_i$represent the activity concentration and its standard uncertainty, respectively. The pairs were considered compatible when $|\, z_i \,| \leq 1.96$and $p \geq 0.05$. The association between both datasets was evaluated using Spearman's correlation coefficient. In addition, a York regression was applied, considering the uncertainties of both variables and zero correlation between them. The slope was compared with unity and the intercept with zero; confidence intervals and probabilities were calculated using the unrounded parameter values.

To apply the CF–CS model, ln(^{210}Pb$_{ex}$) was plotted against mean mass depth. Owing to the visible change in the profile slope, two common segments were defined for both laboratories: 0.4–12.7 and 13.6–52.1 g cm^{-2}. This division was kept identical to avoid selecting different intervals for each dataset. A weighted linear regression was applied to each segment, using $w_i = 1/u^2_{\ln A,i}$as weights. Goodness of fit was evaluated using [20]:

$$\chi^2 = \sum_{i=1}^{n} \frac{(y_i - \hat{y}_i)^2}{u^2_{y_i}},\ \chi^2_\nu = \frac{\chi^2}{n-2} \qquad (5)$$

The value of $p \geq 0.05$ was interpreted as an absence of statistical evidence of lack of fit, but not as proof that the model was fulfilled. The slopes obtained by the two laboratories were compared using a two-sided z-test [9]:

$$z = \frac{m_{\mathrm{LAB}} - m_{\mathrm{IAEA}}}{\sqrt{u^2_{m,\mathrm{LAB}} + u^2_{m,\mathrm{IAEA}}}} \qquad (6)$$

The mass accumulation rates (MAR) and sediment accumulation rates (SAR) were calculated from the slopes with respect to mass depth (m_M) and linear depth (m_z), respectively [19]:

$$\mathrm{MAR} = \frac{\lambda}{|\, m_M \,|},\ \mathrm{SAR} = \frac{\lambda}{|\, m_z \,|} \qquad (7)$$

where $\lambda = 0.03114$ yr^{-1}is the decay constant of ^{210}Pb. The uncertainties were estimated by first-order propagation:

$$u(\mathrm{MAR}) = \mathrm{MAR}\frac{u(m_M)}{|\, m_M \,|},\ u(\mathrm{SAR}) = \mathrm{SAR}\frac{u(m_z)}{|\, m_z \,|} \qquad (8)$$

neglecting the uncertainty in λ. The rates obtained by both laboratories were compared using the same z-test, based on the unrounded values.

RESULTS AND DISCUSSION

Identification of thermal gradients

An essential step before initiating the digestion of samples intended for the estimation of ^{210}Pb activity concentration by alpha spectrometry is to ensure the thermal homogeneity of the hotplate or, failing that, to identify possible heterogeneities in its surface temperature. For this purpose, Fig. 5 presents a two-dimensional map of the surface temperature obtained from systematic measurements in the different sections of the hotplate, which reveals clearly heterogeneous thermal pattern across the surface of the hotplate.

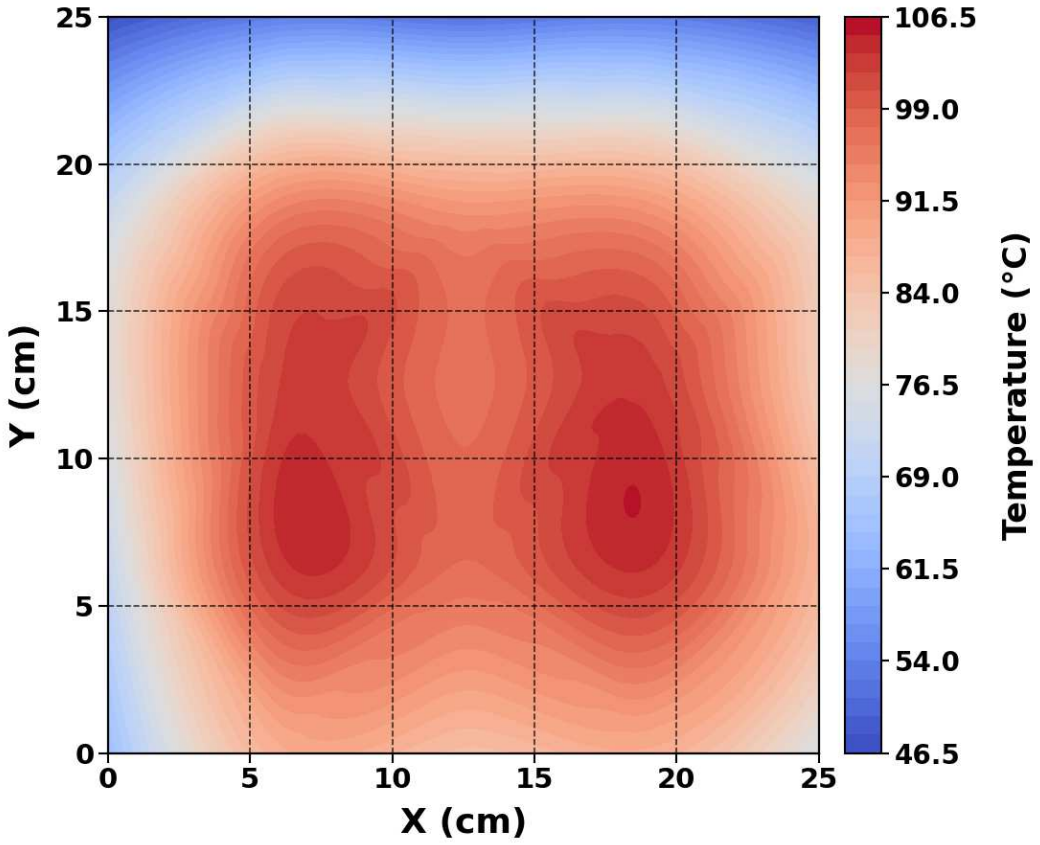


Fig. 5. Two-dimensional map of the surface temperature distribution (°C) of the IKA C-MAG HP 10 hotplate. The color scale represents the spatial distribution of temperature across the heating surface.

The highest temperatures were concentrated mainly in the inner regions of the heating surface, approximately between X = 5–20 cm and Y = 5–20 cm, where values ranging from 91.3 to 103.6 °C were recorded. Within this region, two areas of higher temperature were observed, located approximately around X = 7.5 cm and X = 18 cm, with temperatures close to or above 100 °C. In contrast, a progressive decrease in temperature was observed toward the periphery of the surface. This decrease was more pronounced toward the upper edge (Y = 20–25 cm), where the lowest temperatures were recorded, with minimum values of approximately 47.1–51.7 °C. The lateral edges and areas near the corners also showed temperatures lower than those observed in the inner regions, predominantly within the range of 71–88 °C. Overall, the thermal map reveals a spatial temperature gradient from the inner regions toward the edges of the hotplate, with greater thermal uniformity in the central region and decreasing temperature toward the periphery.

The one-way analysis of variance showed statistically significant differences among the mean temperatures of the three evaluated zones ($p = 9.09 \times 10^{-7}$). Therefore, the null hypothesis of equality of means was rejected, and it was concluded that at least one of the zones had a different mean temperature. Because no subsequent multiple comparisons were performed, the ANOVA result does not allow statistical identification of which pairs of zones differed from each other. Nevertheless, the thermal map and descriptive statistics showed that the central region had temperatures closer to the set value and lower dispersion than the peripheral regions.

Additionally, the spatial temperature differences observed in the two-dimensional map were examined using the box plot presented in Fig. 6 to compare the distribution, central tendency, and dispersion of the temperatures recorded in each zone. As shown in Fig. 6, the central zone exhibited the highest temperatures, with a mean of 98.08 °C and a median of 97.20 °C, while the central 50% of the data ranged from 93.70 to 103.00 °C (Q1–Q3). Group 1 showed intermediate values, with a mean of 79.06 °C, a median of 83.60 °C, and an interquartile range between 77.00 and 87.23 °C. In contrast, Group 2 recorded the lowest temperatures and the greatest dispersion, with a mean of 61.33 °C, a median of 59.20 °C, and Q1 and Q3 values of 53.13 and 71.43 °C, respectively.

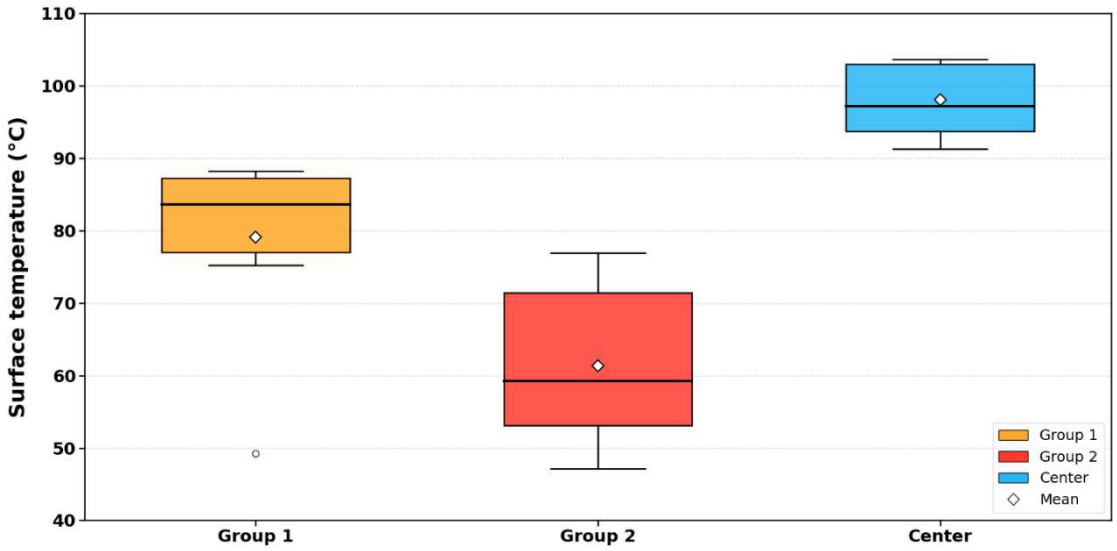


Fig. 6. Box plots for the hotplate groups at 100 °C (IKA C-MAG HP 10 hotplate). The central horizontal line represents the median, the height of the box corresponds to the interquartile range (Q1–Q3), and the whiskers show the data range. The diamond indicates the arithmetic mean of each group, and the individual points represent outliers.

Overall, the descriptive statistics revealed differences in the thermal distribution among the evaluated zones. The central region showed the lowest temperature dispersion, followed by Group 1, whereas Group 2 exhibited the greatest variability. This behavior was consistent with the spatial pattern observed in the two-dimensional temperature map.

Consequently, the central region of the hotplate was selected for positioning the vessels during digestion because it exhibited surface temperatures closer to the set value of 100 °C and lower spatial variability. This selection reduced the potential variability associated with the position of the vessels on the heating surface. However, because the characterization was performed at 100 °C without vessels, samples, or reagents, the results describe only the surface temperature distribution of the hotplate under the test conditions and do not directly represent the internal temperature reached by the mixtures during digestion at 150 °C. Therefore, this test was used

as an operational criterion for selecting the most uniform region of the hotplate and was not considered a measurement of the effective digestion temperature. This control represents a relevant aspect of the analytical procedure because selecting a more thermally uniform surface region may promote greater reproducibility in vessel positioning and heating.

Instrumental background and blanks used in the ^{210}Pb analysis

A fundamental step before measuring ^{210}Po activity concentrations is determining the background of the measurement system (ALPHA DUO alpha spectrometer, ORTEC AMETEK). The samples were measured until approximately 400 counts were reached, corresponding to a relative uncertainty of 5%. On average, the measurement times were 3 days for the upper sections and 8 days for the lower sections. Consequently, a measurement time of 8 days was used to determine the background. Background measurement makes it possible to characterize the statistical fluctuations of the detection system and provides the basis for estimating the detection limit (L_D). This represents the minimum true net signal that can be detected with specified probabilities of committing false-positive and false-negative errors. The detection limit, expressed in net counts, was calculated using the Currie approximation [21]:

$$L_D = 2.71 + 4.65\sqrt{B} \qquad (9)$$

where L_D is the detection limit expressed in net counts and B is the number of background counts recorded over a measurement time equal to that used for the sample. This expression corresponds to type I and type II error probabilities of 0.05 ($\alpha = \beta = 0.05$). Under the normal approximation to the Poisson distribution, the value 2.71 is related to k^2, whereas the coefficient 4.65 incorporates the one-sided normal quantile $k = 1.645$ and the combined variability associated with sample and background counting. The background count rates ranged from 0.34 to 2.04 counts d^{-1} in the ^{210}Po region of interest and from 0.91 to 3.40 counts d^{-1} in the ^{209}Po region (Table 1). All values were below the acceptance criterion of 24 counts d^{-1} established in the equipment manual [22]. Detector 3 showed the highest background count rates in both regions of interest, with 2.04 ± 0.48 counts d^{-1} for ^{210}Po and 3.40 ± 0.62 counts d^{-1} for ^{209}Po. The latter value represented approximately 14% of the limit established by the manufacturer.

Table 1. Characterization of the measurement-system background and equipment detection limits.

Detector	^{210}Po L_D(counts)	^{209}Po L_D(counts)	^{210}Po count rate (counts d^{-1})	^{209}Po count rate (counts d^{-1})
1	13	16	0.57 ± 0.25	0.91 ± 0.32
2	11	24	0.34 ± 0.20	2.38 ± 0.52
3	22	28	2.04 ± 0.48	3.40 ± 0.62
4	12	17	0.45 ± 0.23	1.13 ± 0.36

The analytical blanks showed apparent ^{210}Po activity concentrations on the order of 10^{-4} Bq kg^{-1}, with a mean of $(0.50 \pm 0.25) \times 10^{-4}$ Bq kg^{-1}. In several cases, the values were comparable to their associated uncertainties and several orders of magnitude lower than the minimum detectable activities (MDAs) of the detectors (Table 2). This indicates a low contribution from the reagents and preparation stages susceptible to introducing contamination, such as digestion,

evaporation, transfers, and spontaneous deposition onto silver [6,7]. Potential polonium losses were evaluated independently through the recovery of the ^{209}Po tracer. The MDAs of the four detectors ranged from 0.22 to 0.46 Bq kg^{-1}. Detector 3 exhibited the highest value, consistent with its higher background count rate. Nevertheless, all MDAs were lower than the activities determined in the sediment samples, demonstrating that the sensitivity of the system was adequate for the analyzed range.

Table 2. Results of the analytical blanks for the determination of ^{210}Pb through the measurement of ^{210}Po by alpha spectrometry and estimation of the minimum detectable activity (MDA).

Sample code	Blank activity concentration (×10^{-4} Bq kg^{-1})	Detector	MDA of ^{210}Po (Bq kg^{-1})
Blank R1	1.40 ± 0.66		
Blank R2	0.07 ± 0.33	1	0.27
Blank R3	0.98 ± 0.43		
Blank R4	0.20 ± 0.49	2	0.22
Blank R5	0.33 ± 0.30		
Blank R6	0.02 ± 0.21	3	0.46
Mean	0.50 ± 0.25	4	0.25

Overall, these results validate the application of background corrections and ensure the reliability of the activity concentrations determined in the sediment samples analyzed.

Quality control of the ^{210}Pb analysis

The IAEA-412 reference material was analyzed through ten independent determinations to evaluate the agreement and repeatability of the procedure in a sedimentary matrix. The individual results were compared with the reference value corrected for radioactive decay to the measurement date, corresponding to November 18, 2025 (Table 3). The activity concentrations obtained ranged from 71.00 ± 5.00 to 83.30 ± 5.90 Bq kg^{-1}. The absolute relative differences with respect to the reference value ranged from 0.03 to 9.00%; therefore, all ten determinations met the adopted criterion of an absolute relative difference ≤10%. The ζ-scores ranged from −0.96 to 1.05 and, in all cases, the condition $|\zeta| \leq 2$ was met. This indicates that the experimental results were compatible with the reference value, considering the associated standard uncertainties.

Table 3. Results of the quality control of the procedure for the indirect determination of ^{210}Pb by alpha spectrometry of ^{210}Po in the IAEA-412 reference material

Code	Measured activity (Bq kg^{-1})	Reference activity (Bq kg^{-1})	Absolute relative difference (%)	ζ
IAEA-412-R1	79.80 ± 5.80	76.50 ± 2.80	4.32	0.52
IAEA-412-R2	81.20 ± 6.00	76.50 ± 2.80	6.22	0.72
IAEA-412-R3	76.40 ± 5.60	76.50 ± 2.80	0.03	0.00

IAEA-412-R4	71.90 ± 5.20	76.50 ± 2.80	5.93	-0.77
IAEA-412-R5	76.50 ± 3.80	76.50 ± 2.80	0.03	0.00
IAEA-412-R6	72.70 ± 4.10	76.50 ± 2.80	4.89	-0.76
IAEA-412-R7	77.70 ± 3.90	76.50 ± 2.80	1.62	0.26
IAEA-412-R8	74.20 ± 4.90	76.50 ± 2.80	2.89	-0.39
IAEA-412-R9	83.30 ± 5.90	76.50 ± 2.80	9.00	1.05
IAEA-412-R10	71.00 ± 5.00	76.50 ± 2.80	7.19	-0.96
Mean	76.47 ± 2.94[a]	76.50 ± 2.80	0.03	0.01

Note: The uncertainties of the individual determinations and the reference value were treated as standard uncertainties ($k = 1$). [a]The value reported for the mean corresponds to the 95% confidence interval ($n = 10$).

The mean activity concentration was 76.47 Bq kg^{-1}, with a repeatability standard deviation (s_r) of 4.11 Bq kg^{-1} and a relative standard deviation (RSD) of 5.37%. The 95% confidence interval for the mean was 76.47 ± 2.94 Bq kg^{-1} ($n = 10$), in agreement with the corrected reference value of 76.50 ± 2.80 Bq kg^{-1}. The absolute bias was 0.03 Bq kg^{-1}, the relative bias was 0.04%, and the recovery relative to the reference value was 99.96%. Overall, these results provided evidence of satisfactory agreement and repeatability for the reference material and the analytical conditions evaluated.

Chemical recovery of the tracer in the ^{210}Pb analysis

The chemical recovery (R) was calculated from the activity of the added tracer, the net count rate of the corresponding peak, and the detection efficiency (ε). Although recovery is not directly required to calculate the activity concentration in isotope-dilution alpha spectrometry, its determination made it possible to evaluate the overall performance of the analytical procedure and verify the absence of significant losses or systematic biases during the different stages of the radiochemical treatment. Recovery was estimated according to the following expression [8]:

$$R = \frac{R_{GT} - R_{BT}}{A_T \cdot m_T \cdot \varepsilon \cdot \exp(\lambda_T t_T)} \qquad (10)$$

where R_{GT} and R_{BT}correspond to the tracer and background count rates in the ^{209}Po region of interest, respectively; A_T is the specific activity of the added tracer; m_T, the mass of tracer added; ε, the detection efficiency; and λ_T, the decay constant of the tracer for an elapsed time t_T. The uncertainty in recovery was obtained by propagating the standard uncertainties of the variables involved.

The ^{209}Po chemical-recovery graph shows that the values obtained during application of the analytical procedure ranged approximately from 61 to 79% (Fig. 7). The mean recovery was 73 ± 4%, where $\sigma = 4\%$ corresponds to the standard deviation of the determinations. The lines corresponding to the mean ± 2σ defined an approximate interval from 65.30 to 80.40%, within

which most of the determinations were located. Some recoveries below this interval were observed, particularly values close to 61–62%. In general, the recovery values were distributed around the mean, although some determinations fell outside the interval defined by ± 2σ. The error bars associated with each point represent the uncertainties corresponding to the individual chemical recoveries. The variability observed in ^{209}Po recovery may be associated with the cumulative yield of the different stages that comprise the radiochemical procedure. During sample preparation, partial polonium losses may occur during stages such as digestion of the sedimentary matrix, transfers between vessels, subsequent chemical treatments, and, finally, the spontaneous deposition of Po onto silver discs. Consequently, a recovery below 100% does not necessarily imply inadequate performance of the procedure but rather reflects the fraction of the tracer that was effectively recovered and quantified after completion of all analytical stages. Differences among determinations may be related to small variations in these experimental stages and to the specific conditions of each sample.

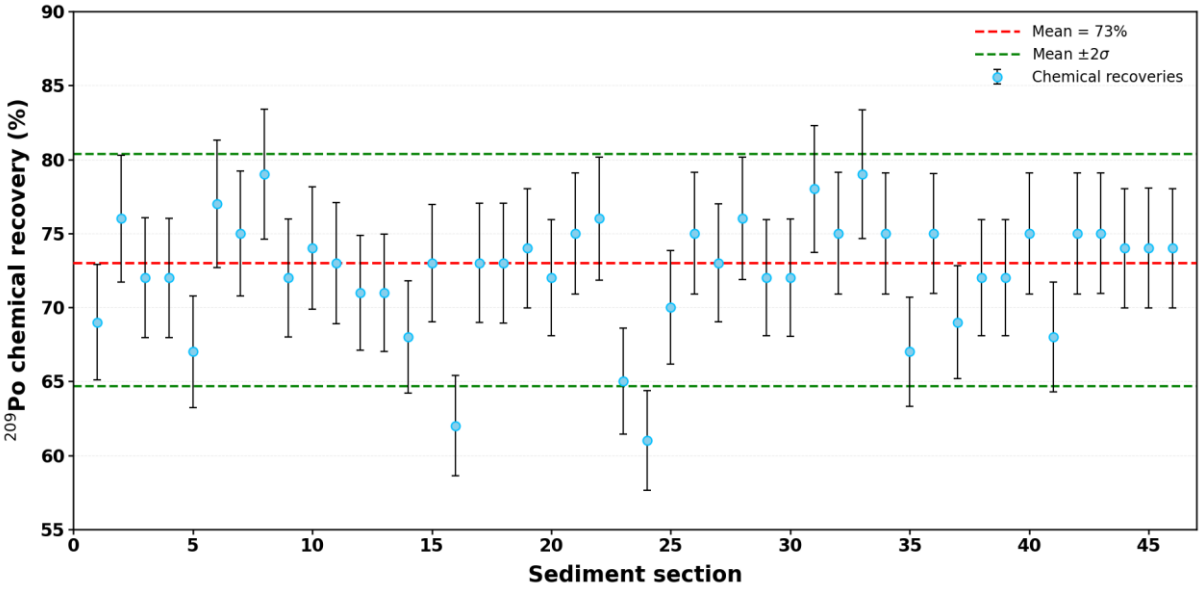


Fig. 7. Chemical recovery of the ^{209}Po tracer for the sediment sections analyzed. The points and error bars represent the individual recoveries and their associated uncertainties, respectively. The dashed red line indicates the mean recovery (73%), and the dashed green lines correspond to the mean ± 2 SD. The coefficient of variation of the recoveries was approximately 5%.

Recovery below 100% may be related to the cumulative yield of digestion, evaporation, transfers, and spontaneous polonium deposition onto silver discs [6, 7]. However, in an isotope-dilution procedure, quantitative recovery is not essential, provided that the tracer is added before the critical stages, its recovery is determined individually, and ^{209}Po and ^{210}Po exhibit equivalent chemical behavior [16]. In this study, the stability of the recoveries and their low relative dispersion support the consistency of the radiochemical preparation. Individual losses were corrected using the ^{209}Po tracer, whereas the lower recoveries were reflected mainly in increased counting times and associated uncertainties.

^{210}Pb activity concentration in sediment core ELS7011-BJ-Z3N5

The activity concentration of ^{210}Pb in samples from the ELS7011-BJ-Z3N5 sediment core was determined at LABTOX-UES by alpha spectrometry (ALPHA DUO, AMETEK ORTEC) through measurement of its daughter radionuclide ^{210}Po, assuming radioactive equilibrium between the two radionuclides. The total ^{210}Pb profiles obtained by LABTOX-UES and IAEA-MEL are presented in Fig. 8A. Activity concentrations determined by LABTOX-UES ranged from 14.00 to 31.40 Bq kg^{-1}, whereas those obtained by IAEA-MEL ranged from 15.30 to 32.30 Bq kg^{-1}. In both profiles, activity generally decreased with increasing depth. The absolute uncertainties associated with the activity concentrations determined by both laboratories ranged from 0.70 to 2.10 Bq kg^{-1}. In relative terms, uncertainties ranged from approximately 3.30 to 6.80% for IAEA-MEL and from 4.90 to 7.00% for LABTOX-UES, showing similar ranges of relative uncertainty for the two sets of measurements.

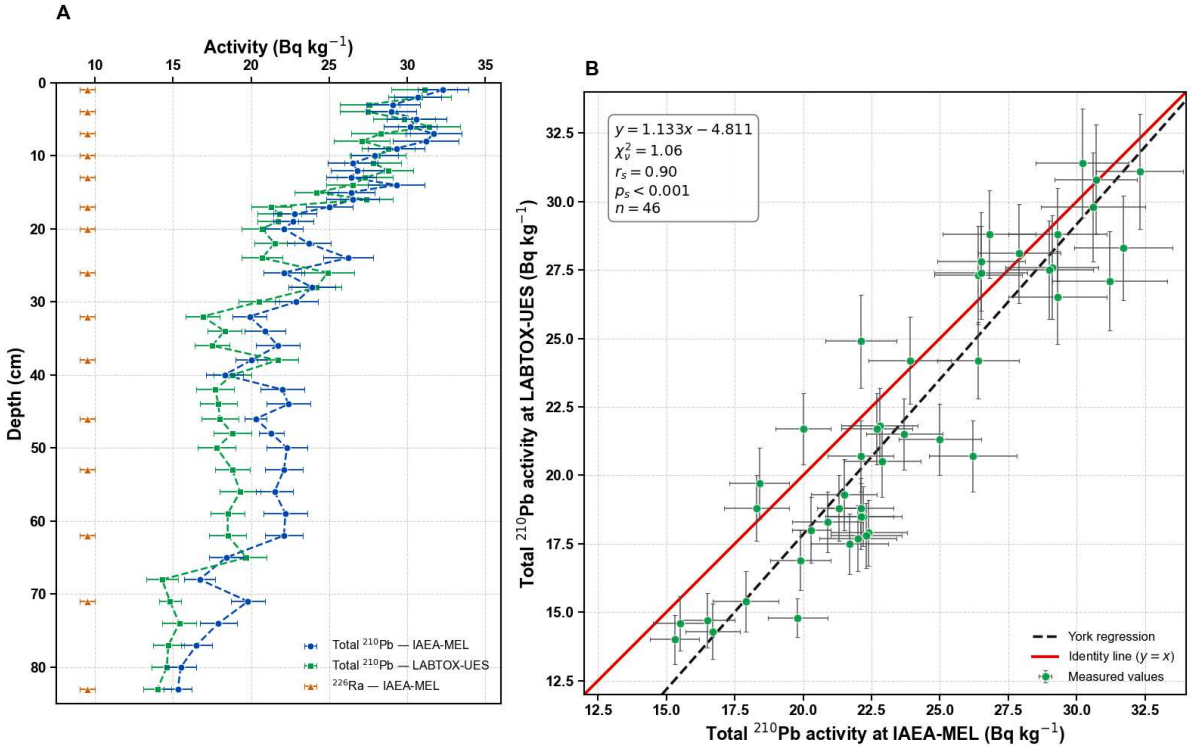


Fig. 8. Comparison of total ^{210}Pb activity concentrations in core ELS7011-BJ-Z3N5 determined by IAEA-MEL and LABTOX-UES: (A) vertical profiles and (B) linear regression between laboratories.

The ^{226}Ra activity concentrations were determined in five sections distributed between 5 and 46 cm depth. The values ranged from 7.87 ± 0.06 to 10.21 ± 0.46 Bq kg^{-1}. The mean activity was 9.52 ± 0.49 Bq kg^{-1}, where the value reported after the ± sign corresponds to the 68% confidence interval for the mean, calculated using the student's t-distribution ($n = 5$). The standard deviation among the sections was 0.97 Bq kg^{-1}, equivalent to an RSD of 10.16%. The uncertainties of excess ^{210}Pb were obtained by propagating the standard uncertainties associated with the total ^{210}Pb and ^{226}Ra activities and were subsequently propagated to calculate the uncertainty of ln(^{210}Pb$_{ex}$) used in the weighted regressions.

The linear regression between ^{226}Ra activity concentration and depth showed no significant trend ($r = 0.25$; $p = 0.69$). Because no systematic variation with depth was observed, the mean value of 9.52 Bq kg^{-1} was used as a constant estimator of supported ^{210}Pb activity in all

46 core sections. Nevertheless, this approximation should be interpreted considering that only five core sections were analyzed by gamma spectrometry.

Table 4. ^{226}Ra activity concentrations determined from the ^{214}Pb gamma lines in five sections of core ELS7011-BJ-Z3N5.

Depth (cm)	Mass (g)	Time (days)	^{226}Ra (Bq kg^{-1})
5	5.4384	3.03	10.21 ± 0.46
16	5.7546	1.96	7.87 ± 0.06
26	5.9179	6.02	9.48 ± 0.07
36	5.8411	1.25	10.17 ± 1.44
46	5.8217	1.97	9.86 ± 1.04
Media	—	—	9.52 ± 0.49[a]

[a]68% confidence interval of the mean calculated using Student's t-distribution ($n = 5$). The standard deviation among the sections was 0.97 Bq kg^{-1}.

Compatibility was assessed for each measurement pair using a z-test that incorporated the uncertainties of both results. Of the 46 pairs, 37 (80.4%) did not differ significantly ($p > 0.05$; $|z| < 1.96$), indicating that the LABTOX-UES and IAEA-MEL results were compatible within their reported analytical uncertainties for most sections. No significant differences occurred between 1 and 20 cm. The remaining nine pairs (19.6%) differed significantly ($p < 0.05$; $|z| > 1.96$) at depths of 24, 36, 42, 44, 50, 53, 59, 62, and 71 cm. In every case, LABTOX-UES reported lower activity concentrations than IAEA-MEL. This consistent direction may indicate a negative bias in some sections.

Subsequently, the linear relationship between the activity concentrations determined by both laboratories was evaluated (Fig. 8B). As a first step, Spearman's correlation test was applied, which showed a strong, positive, and statistically significant monotonic association between both sets of measurements ($r_s = 0.90$; $p < 0.001$; $n = 46$). This result indicates that the two laboratories reproduced the variation in ^{210}Pb activity along the core in a similar manner; that is, sections with high activities at IAEA-MEL also tended to exhibit high activities at LABTOX-UES, and vice versa. A York regression was also applied [23], considering the activity concentrations determined by IAEA-MEL as the independent variable and those obtained by LABTOX-UES as the dependent variable. This fit incorporated the individual uncertainties associated with the measures from both laboratories. The resulting equation was:

$$A_{\mathrm{LABTOX-UES}} = (1.133)\, A_{\mathrm{IAEA-MEL}} - 4.811 \qquad (11)$$

The activity concentrations and intercept are expressed in Bq kg^{-1}, whereas the slope is dimensionless. The estimated slope was b = 1.133 ± 0.070 (standard uncertainty, k = 1), with an approximate 95% confidence interval ranging from 0.995 to 1.271. Although the estimated slope deviated from unity by approximately 13.3%, this difference was not statistically significant ($p \approx 0.060$, two-sided test using a normal approximation). Therefore, the slope was compatible with unity within the uncertainty of the fit. However, this result alone does not demonstrate equality between the measurements obtained by the two laboratories.

The intercept was negative, and its approximate 95% confidence interval excluded zero (a = −4.81 ± 1.57 Bq kg^{-1}, standard uncertainty, k = 1; 95% CI: −7.89 to −1.73 Bq kg^{-1}; $p = 0.0022$, two-sided test using a normal approximation). Furthermore, the fitted line lay below the identity line (Y = X) over the range of IAEA-MEL activity concentrations examined, from 15.3 to 32.3

Bq kg^{-1}. This behavior indicates a tendency for LABTOX-UES to obtain lower activity concentrations than IAEA-MEL. This interpretation is consistent with the observed mean difference between the two measurement datasets of −1.67 Bq kg^{-1} and the mean symmetric relative difference of −8.15%. Nevertheless, the intercept should be interpreted cautiously because it represents the predicted value when the IAEA-MEL activity concentration is zero, which lies outside the experimental range.

The fit yielded a reduced chi-square value close to unity (χ^2_{red} = 1.06) and a goodness-of-fit p-value of 0.371 (χ^2 = 46.48, ν = 44 degrees of freedom). Under the assumptions of normally distributed errors, independent measurement pairs, and uncorrelated errors between the two laboratories within each pair (r_i = 0), these results indicate that the scatter around the fitted line is compatible with the analytical uncertainties considered, with no statistically significant evidence of lack of fit. Nevertheless, the distribution of the points relative to the identity line shows that the differences between the laboratories varied among the sections.

Estimation of mass accumulation and sediment accumulation rates using the CF–CS model

From the activity concentrations obtained, excess ^{210}Pb was estimated as the difference between total ^{210}Pb and ^{226}Ra activities, using the latter as an estimator of supported ^{210}Pb under the assumption of secular equilibrium. Subsequently, the distribution of ln(^{210}Pb$_{ex}$) as a function of cumulative mean mass depth was examined according to the constant flux–constant sedimentation (CF–CS) model described by Sánchez-Cabeza et al. [19].

The profile showed two intervals with distinct linear behaviors; therefore, a segmented fit was applied independently to the activities determined by LABTOX-UES and IAEA-MEL. The first segment corresponded to the surface interval, where the most pronounced decrease in excess ^{210}Pb activity was observed, whereas the second comprised the subsurface and deep sections, which were characterized by a more gradual decrease. For each section, the natural logarithm of the excess ^{210}Pb activity concentration was calculated and plotted as a function of cumulative mean mass depth. The mass depth of each section was determined from its dry mass and the cross-sectional area of the core, whereas the mean mass depth was calculated as the midpoint between the upper and lower mass-depth boundaries of each interval. Similarly, the mean linear depth was established as the midpoint between the upper and lower boundaries of each sediment section. The fits obtained for both sets of measurements are presented in Fig. 9.

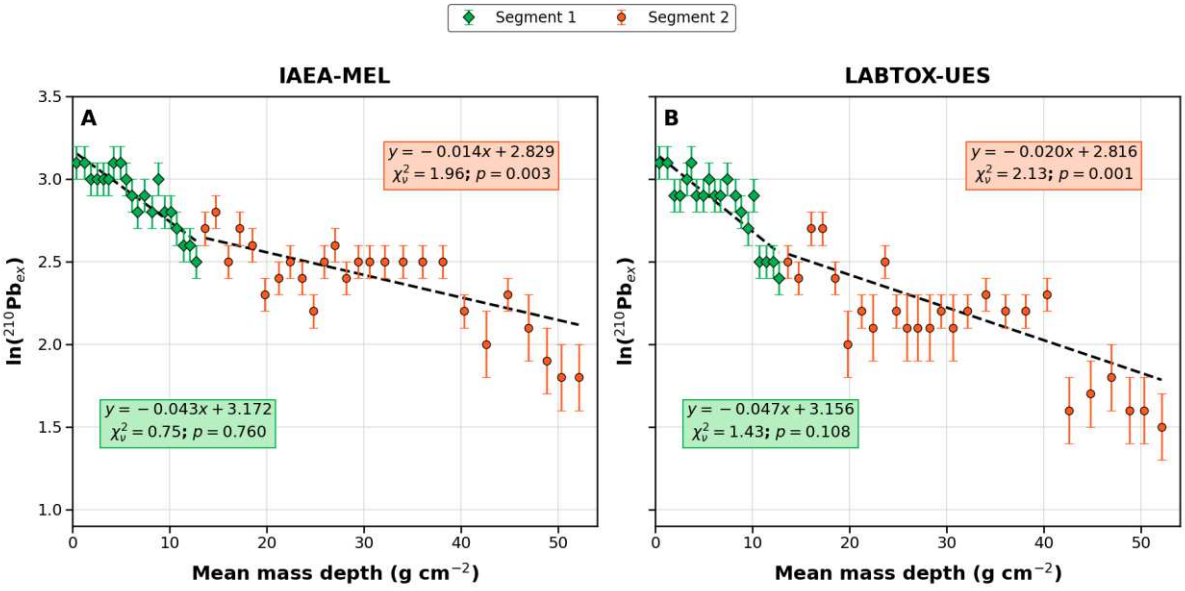


Fig. 9. Segmented weighted linear regressions of ln(^{210}Pb$_{ex}$) as a function of mean cumulative mass depth for the activity concentrations determined by IAEA-MEL (C) and LABTOX-UES (D).

The relationships between ln($^{210}Pb_{ex}$) and mass depth showed negative slopes in both datasets, consistent with the decrease in excess ^{210}Pb activity toward the deeper core sections. Because the observations had different uncertainties, the parameters were estimated using weighted linear regressions, with the inverse of the variance of ln($^{210}Pb_{ex}$) used as weights. In the first segment, the slopes obtained for IAEA-MEL and LABTOX-UES were −0.043 ± 0.006 and −0.047 ± 0.006 cm² g⁻¹, respectively, whereas the intercepts were 3.172 ± 0.046 and 3.156 ± 0.046. Although the slope estimated for LABTOX-UES was approximately 9.30% greater in magnitude, the difference between the two slopes was not statistically significant ($z = -0.52$; $p = 0.602$). This suggests that both datasets described comparable excess ^{210}Pb decrease gradients within this interval.

Goodness of fit was evaluated using the chi-square statistic. For the first segment, values of $\chi^2_\nu = 0.75$and $p = 0.760$were obtained for IAEA-MEL, and $\chi^2_\nu = 1.43$ and $p = 0.108$for LABTOX-UES. In both cases, the p-values were greater than 0.05; therefore, insufficient statistical evidence was found to reject the linear relationship, considering the analytical uncertainties used. Likewise, the paired comparison between the results from both laboratories yielded $\chi^2_\nu = 0.68$and $p = 0.855$, indicating that the differences observed in this segment were, overall, compatible with the standard uncertainties.

In the second segment, the weighted slopes were less steep, with values of −0.014 ± 0.002 cm² g⁻¹ for IAEA-MEL and −0.020 ± 0.002 cm² g⁻¹ for LABTOX-UES. The lower magnitude of these slopes compared with those obtained in the first segment represents a more gradual decrease in ln($^{210}Pb_{ex}$) with increasing mass depth. The difference between the slopes approached the conventional significance level, although it was not statistically significant ($z = -1.91$; $p = 0.056$).

Despite the decreasing trend, the reduced chi-square values for the second segment were $\chi^2_\nu = 1.96$for IAEA-MEL and $\chi^2_\nu = 2.13$ for LABTOX-UES, with probabilities of $p = 0.0034$ and $p = 0.0010$, respectively. These results indicate that the dispersion of the activities around the fitted lines was greater than expected based on the analytical uncertainties. In addition, the paired comparison between laboratories showed limited compatibility within this interval ($\chi^2_\nu = 2.63$; $p < 0.001$). Therefore, the interpretation of the second segment under the assumptions of constant flux and constant accumulation should be made with caution.

The slopes of the first segment, whose fits were compatible with the analytical uncertainties, were used to estimate the mean mass accumulation and sediment accumulation rates using the CF–CS model. MAR was calculated from the slope of ln($^{210}Pb_{ex}$) with respect to mass depth, whereas SAR was estimated using the slope corresponding to mean linear depth. The results obtained for both laboratories and their comparison using a z-test are presented in Table 5.

Table 5. Comparison of the mean mass accumulation and sediment accumulation rates estimated from the IAEA-MEL and LABTOX-UES results.

Parameter	IAEA-MEL	LABTOX-UES	Absolute difference	z	p
MAR (g cm^{-2} year^{-1})	0.72 ± 0.10	0.66 ± 0.08	0.07	0.52	0.61
SAR (cm year^{-1})	1.14 ± 0.16	1.03 ± 0.13	0.11	0.50	0.62

As shown in Table 5, the rates estimated from the IAEA-MEL results were nominally higher than those obtained using the LABTOX-UES data. The absolute differences, calculated using the unrounded values, were 0.07 g cm^{-2} yr^{-1} for the mass accumulation rate and 0.11 cm yr^{-1} for the sediment accumulation rate. However, the two-sided *z*-test showed no statistically significant differences for either MAR ($z = 0.52$; $p = 0.61$) or SAR ($z = 0.50$; $p = 0.62$). In both cases, the absolute *z* values were below the critical value of 1.96, and the probabilities were greater than 0.05; therefore, the observed differences were compatible with the combined standard uncertainties.

Overall, the similarity between the weighted slopes of the first segment, the absence of significant differences between the rates, and the results of the goodness-of-fit tests suggest general consistency between the estimates derived from the two datasets. Nevertheless, these results do not demonstrate that the rates are identical, but rather that the observed differences were not sufficiently large relative to their uncertainties to establish a statistically significant difference. In contrast, the lack of fit identified in the second segment limits the interpretation of the rates that could be derived from that interval; therefore, it was considered more appropriate to use only the first segment to estimate and compare MAR and SAR.

Conclusions

The adapted procedure allowed the indirect determination of ^{210}Pb activity by alpha spectrometry of ^{210}Po under controlled analytical conditions. The low blank contribution, minimum detectable activities of 0.22–0.46 Bq kg^{-1}, relatively stable chemical recovery of the ^{209}Po tracer (73 ± 4 %), and agreement obtained for the IAEA-412 material provided evidence of satisfactory performance for the matrix and conditions evaluated. However, because the activity of the reference material was higher than that observed in the samples, these results alone do not constitute complete validation over the entire concentration range analyzed.

The interlaboratory comparison showed that 37 of the 46 pairs of results (80.4 %) were statistically compatible and that the slope of the York regression was compatible with unity. Nevertheless, the negative intercept and the lower concentrations obtained by LABTOX-UES in nine sections preclude establishing complete analytical equivalence between the two laboratories. In the surface segment, the MAR and SAR estimates did not differ significantly, supporting the application of the procedure to estimate recent sediment accumulation rates; however, the lack of fit in the deep segment limits the application of the CF–CS model within that interval.

Funding

This research received financial and in-kind support through Project ELS7011, “Strengthening national capacities for sustainable environmental management in the context of climate change.” The International Atomic Energy Agency (IAEA) funded the project and donated laboratory equipment used in this study. The Salvadoran Water Authority (ASA) funded laboratory consumables. The Marine Toxins Laboratory of the University of El Salvador (LABTOX-UES) provided laboratory facilities and access to equipment, while the Ministry of Environment and Natural Resources (MARN) supported field sampling by providing boats and fuel. No additional funding was received specifically for manuscript preparation or publication.

References

1. Bernal JP, Beramendi Orosco LE, Lugo-Ibarra KC, Daesslé LW (2010) Revisión a algunos geocronómetros radiométricos aplicables al Cuaternario. Bol Soc Geol Mex 62:305–323. https://doi.org/10.18268/BSGM2010v62n3a1

2. Krishnaswamy S, Lal D, Martin JM, Meybeck M (1971) Geochronology of lake sediments. Earth Planet Sci Lett 11:407–414. https://doi.org/10.1016/0012-821X(71)90202-0

3. Appleby PG (2001) Chronostratigraphic techniques in recent sediments. In: Last WM, Smol JP (eds) Tracking environmental change using lake sediments, vol 1: Basin analysis, coring, and chronological techniques. Kluwer Academic Publishers, Dordrecht, pp 171–203. https://doi.org/10.1007/0-306-47669-X_9

4. Arias-Ortiz A, Masqué P, Garcia-Orellana J, Serrano O, Mazarrasa I, Marbà N, Lovelock CE, Lavery PS, Duarte CM (2018) Reviews and syntheses: ^{210}Pb-derived sediment and carbon accumulation rates in vegetated coastal ecosystems—setting the record straight. Biogeosciences 15:6791–6818. https://doi.org/10.5194/bg-15-6791-2018

5. Ren H, Gong X, Zhou L, Wang P, Cao Y (2024) Recent progresses in analytical method development for ^{210}Pb in environmental and biological samples. Environ Sci Pollut Res 31:31664–31678. https://doi.org/10.1007/s11356-024-33272-3

6. Matthews KM, Kim CK, Martin P (2007) Determination of ^{210}Po in environmental materials: a review of analytical methodology. Appl Radiat Isot 65:267–279. https://doi.org/10.1016/j.apradiso.2006.09.005

7. Flynn WW (1968) The determination of low levels of polonium-210 in environmental materials. Anal Chim Acta 43:221–227. https://doi.org/10.1016/S0003-2670(00)89210-7

8. Vajda N, Pöllänen R, Martin P, Kim CK (2020) Alpha spectrometry. In: L'Annunziata MF (ed) Handbook of radioactivity analysis, 4th edn, vol 1: Radiation physics and detectors. Academic Press, pp 493–573. https://doi.org/10.1016/B978-0-12-814397-1.00005-4

9. Joint Committee for Guides in Metrology (2008) Evaluation of measurement data—Guide to the expression of uncertainty in measurement. JCGM 100:2008. Bureau International des Poids et Mesures, Sèvres. https://doi.org/10.59161/JCGM100-2008E

10. Cuesta E, Barba-Lobo A, Lozano RL, San Miguel EG, Mosqueda F, Bolívar JP (2022) A comparative study of alternative methods for ^{210}Pb determination in environmental samples. Radiat Phys Chem 191:109840. https://doi.org/10.1016/j.radphyschem.2021.109840

11. Dulanská S, Silliková V, Burganová A, Bujdoš M, Trnka M, Kosnáč D, Pánik J (2024) Comparative analysis of AnaLig Sr01 and Sr Resin methods for ^{210}Pb determination in tobacco using TriCarb 3100 TR spectrometry: a statistical approach to accuracy and efficiency. J Radioanal Nucl Chem 333:5713–5720. https://doi.org/10.1007/s10967-024-09597-1

12. Zaborska A, Carroll J, Papucci C, Pempkowiak J (2007) Intercomparison of alpha and gamma spectrometry techniques used in ^{210}Pb geochronology. J Environ Radioact 93:38–50. https://doi.org/10.1016/j.jenvrad.2006.11.007

13. Garcia-Tenorio R, Rozmaric M, Harms A, De Oliveira Godoy JM, Barsanti M, Schirone A, Ruiz-Fernández AC, Sanchez-Cabeza JA, McGinnity P, Fujak M, Eriksson M, Hatje V, Laissaoui A, Nguyen HQ, Okuku E, Al-Rousan SA, Yii MW, Heijnis H, Osvath I (2020) From radiometry to chronology of a marine sediment core: a ^{210}Pb dating interlaboratory comparison exercise organised by the IAEA. Mar Pollut Bull 159:111490. https://doi.org/10.1016/j.marpolbul.2020.111490

14. Barsanti M, Garcia-Tenorio R, Schirone A, Rozmaric M, Ruiz-Fernández AC, Sanchez-Cabeza JA, Delbono I, Conte F, De Oliveira Godoy JM, Heijnis H, Eriksson M, Hatje V, Laissaoui A, Nguyen HQ, Okuku E, Al-Rousan SA, Uddin S, Yii MW, Osvath I (2020) Challenges and limitations of the ^{210}Pb sediment dating method: results from an IAEA modelling interlaboratory comparison exercise. Quat Geochronol 59:101093. https://doi.org/10.1016/j.quageo.2020.101093

15. International Atomic Energy Agency (2024) A guide to the use of sediments in reconstructing the pollution history of coastal areas. IAEA-TECDOC-1953. International Atomic Energy Agency, Vienna

16. Masqué P (2017) Determination of ^{210}Pb in sediment samples. RiO5 Method (16), ERL-ECU/LM/0001-01. School of Science, Edith Cowan University

17. Howard J, Hoyt S, Isensee K, Pidgeon E, Telszewski M (eds) (2014) Coastal blue carbon: methods for assessing carbon stocks and emissions factors in mangroves, tidal salt marshes, and seagrass meadows. Conservation International, Intergovernmental Oceanographic Commission of UNESCO, International Union for Conservation of Nature, Arlington, VA

18. Gascón JL, Muñoz A (2003) Optimization of the parameters affecting the solid state detector efficiency in alpha-spectrometry. J Radioanal Nucl Chem 257:371–374. https://doi.org/10.1023/A:1024748232757

19. Sánchez-Cabeza JA, Ruiz-Fernández AC (2012) ^{210}Pb sediment radiochronology: an integrated formulation and classification of dating models. Geochim Cosmochim Acta 82:183–200. https://doi.org/10.1016/j.gca.2010.12.024

20. Bevington PR, Robinson DK (2003) Data reduction and error analysis for the physical sciences, 3rd edn. McGraw-Hill, Boston

21. Currie LA (1968) Limits for qualitative detection and quantitative determination. Application to radiochemistry. Anal Chem 40:586–593. https://doi.org/10.1021/ac60259a007

22. ORTEC (2022) Alpha Duo, Alpha Mega, and Alpha Ensemble integrated alpha spectrometer: hardware user's guide. Part No. 932505, revision G. AMETEK ORTEC. https://www.ortec-online.com/-/media/ametekortec/manuals/a/alpha-duo-mega-ensemble-mnl.pdf. Accessed 2 October 2026

23. York D, Evensen NM, López Martínez M, De Basabe Delgado J (2004) Unified equations for the slope, intercept, and standard errors of the best straight line. Am J Phys 72:367–375. https://doi.org/10.1119/1.1632486